Polarization effects in bound-free pair production

J. Sommerfeldt [1,2] R. A. Müller [1,2] A. N. Artemyev,[3] and A. Surzhykov[1,2]

[1]*Physikalisch-Technische Bundesanstalt, D-38116 Braunschweig, Germany*
[2]*Technische Universität Braunschweig, D-38106 Braunschweig, Germany*
[3]*Institut für Physik und CINSaT, Universität Kassel, D-34132 Kassel, Germany*

We present a theoretical study of bound-free electron-positron pair production in the interaction of γ rays with bare ions. Special attention is paid to the longitudinal polarization of both the emitted positrons and the produced hydrogenlike ions. To evaluate this polarization we employed exact solutions of the relativistic Dirac equation and treat the electron-photon coupling within the framework of first-order perturbation theory. Detailed calculations have been performed for both low- and high-Z ions and for a wide range of photon energies. The results of these calculations suggest that bound-free pair production can be a source of strongly polarized positrons and ions.

I. INTRODUCTION

Owing to the development and construction of novel acceleration facilities such as FAIR in Darmstadt and Gamma-Factory at CERN [1], new interest arises to study high-energy ion-ion and ion-photon collisions. One of the most fundamental processes in these collisions is the creation of electron-positron pairs. The studies of this $e^- e^+$ process have a long history both in experiment and in theory. For example, due to its large cross section the creation of free $e^- e^+$ pairs has been extensively studied in ultrarelativistic ion-ion collisions [2–6]. Bound-free pair production is less probable in the high energy regime but still plays a significant role in accelerator physics since it leads to beam loss in heavy-ion colliders [7,8]. Theoretical analysis of this process can be performed very conveniently within the framework of the equivalent photon method by Weizsäcker and Williams [9,10]. In this approach the analysis of pair production in ion-ion collisions is traced back to its counterpart in photon-ion interactions. The investigation of photon induced pair production also attracts considerable attention since it allows us to gain more valuable information about light-matter interactions in the ultrarelativistic regime [11–14].

A large number of theoretical studies of photoinduced bound-free pair production have been performed during the last couple of decades [15–20]. Most of these studies have been focused on the total and angle-differential cross sections while much less attention has been paid to the polarization of the positrons and residual hydrogenlike ions. Detailed analysis of these polarization properties may help us to gain more insight into electron and positron dynamics in the relativistic regime. With the advance of positron spectrometers and storage ring techniques these studies become feasible, for example, in the FAIR and CERN facilities. In this work, therefore, we present a theoretical investigation of bound-free $e^- e^+$ pair production in collisions of γ-ray photons with fully stripped or *bare* ions. A special emphasis in this study is placed on the polarization of the produced positrons

and hydrogenlike ions. In order to analyze these polarization properties we employ the relativistic Dirac equation to describe electron and positron states and first-order perturbation theory for the coupling to the electromagnetic field. Based on this approach, in Sec. II we derive the transition matrix element which is later used to calculate partial differential cross sections. By making use of these cross sections, we obtain the degree of polarization of the positrons and ions. Evaluation of these degrees of polarization requires high-demanding computations of free-bound integrals involving the radial components of the Dirac states. These computations are discussed in Sec. III. Later in Sec. IV, we show the results of our calculations for interactions of photons in a wide range of energies with bare ions. In particular, we have found that bound-free pair production by circularly polarized light may lead to the production of strongly polarized positrons and residual hydrogenlike ions. Our results are finally summarized in Sec. V. Relativistic units $\hbar = c = m_e = 1$ are used in this paper if not stated otherwise.

II. THEORY

A. Evaluation of the transition amplitude

In relativistic theory, $e^- e^+$ pair production can be described as the excitation of an electron from the Dirac negative-energy continuum. The remaining hole in the Dirac sea corresponds to the produced positron. If during such an excitation the electron is captured into a bound ionic state, one talks about bound-free pair production. Analysis of all properties of this bound-free process can be traced back to the evaluation of the transition matrix element

$$M_{m_s \mu_f}(\lambda) = \int d\boldsymbol{r}\, \psi^\dagger_{n_f \kappa_f \mu_f}(\boldsymbol{r}) \boldsymbol{\alpha} \cdot \hat{\boldsymbol{u}}_\lambda e^{i\boldsymbol{k}\cdot\boldsymbol{r}} \psi^{(+)}_{\boldsymbol{p},m_s}(\boldsymbol{r}), \quad (1)$$

where the coupling to the electromagnetic field is treated in Coulomb gauge and within the framework of first-order perturbation theory. Evaluation of the matrix element (1) requires

explicit representations of the initial- and final-state wave functions, $\psi_{\boldsymbol{p},m_s}^{(+)}(\boldsymbol{r})$ and $\psi_{n_f\kappa_f\mu_f}(\boldsymbol{r})$, as well as the electron-photon interaction operator $\hat{R} = \boldsymbol{\alpha} \cdot \hat{\boldsymbol{u}}_\lambda e^{i\boldsymbol{k}\cdot\boldsymbol{r}}$. The wave function for the final state is given by the usual bound-electron solution of the Dirac equation

$$\psi_{n_f\kappa_f\mu_f}(\boldsymbol{r}) = \begin{pmatrix} g_{n_f\kappa_f}(r)\chi_{\kappa_f}^{\mu_f}(\hat{\boldsymbol{r}}) \\ if_{n_f\kappa_f}(r)\chi_{-\kappa_f}^{\mu_f}(\hat{\boldsymbol{r}}) \end{pmatrix}, \qquad (2)$$

where n_f is the principal quantum number, κ_f is the Dirac quantum number, and μ_f is the projection of the total angular momentum $j_f = |\kappa_f| - \frac{1}{2}$ [21,22]. In our work, this projection is defined with respect to the propagation direction of the incident light, which is chosen as the z axis. Moreover, in Eq. (2), $g_{n_f\kappa_f}(r)$ and $f_{n_f\kappa_f}(r)$ are the large and small radial components and $\chi_{\kappa_f}^{\mu_f}$ denotes the normalized spin-angular function.

In contrast to the bound-state wave function (2), $\psi_{\boldsymbol{p},m_s}^{(+)}(\boldsymbol{r})$ describes an electron in the Dirac negative-energy continuum. In scattering theory it is usually convenient to express this continuum solution as a decomposition into its partial waves. The explicit form of this multipole expansion depends on the choice of the axis along which the spin of the negative continuum electron is quantized. For proper analysis of polarization effects in $e^- e^+$ pair production, this axis has to be taken along the asymptotic momentum $\boldsymbol{p}$. In this so-called helicity representation, the electron wave function reads as

$$\psi_{\boldsymbol{p},m_s}^{(+)}(\boldsymbol{r}) = \sum_{\kappa_i\mu_i} i^{l_i} e^{i\Delta_{\kappa_i}} \sqrt{4\pi(2l_i+1)} \left\langle l_i 0 \frac{1}{2} m_s \middle| j_i m_s \right\rangle$$
$$\times \begin{pmatrix} g_{E\kappa_i}(r)\chi_{\kappa_i}^{\mu_i}(\hat{\boldsymbol{r}}) \\ if_{E\kappa_i}(r)\chi_{-\kappa_i}^{\mu_i}(\hat{\boldsymbol{r}}) \end{pmatrix} D_{\mu_i m_s}^{j_i}(\phi,\theta,0). \qquad (3)$$

Here, m_s denotes the electron spin projection onto the propagation direction and l_i is the orbital angular momentum of the upper component. Furthermore, $D_{\mu_i m_s}^{j_i}(\phi,\theta,0)$ is the Wigner D function, where ϕ and θ denote the azimuthal and polar angle of the electron asymptotic momentum, and

$$\Delta_{\kappa_i} = \delta_{\kappa_i} - \arg\Gamma(s+i\eta) - \frac{1}{2}\pi s + (l_i+1)\frac{\pi}{2} \qquad (4)$$

is the difference between the asymptotic phases of the Dirac-Coulomb and free Dirac solutions.

Equation (3) describes an electron with asymptotic momentum $\boldsymbol{p}$ in the Dirac negative-energy continuum. As already mentioned above, this wave function can be naturally used to describe the emitted positron. Namely, within the picture of the Dirac sea, the creation of an outgoing positron with energy $E_+ > 0$, momentum $\boldsymbol{p}_+$, and helicity m_+ is equivalent to the excitation of an incoming electron with energy $E = -E_+$, momentum $\boldsymbol{p} = -\boldsymbol{p}_+$, and helicity $m_s = m_+$. The radial components of such a negative-energy electron in a Coulomb potential are given by

$$g_{E\kappa_i}(r) = N_{\kappa_i}(|E|-1)^{\frac{1}{2}}(2pr)^{s-1}\mathrm{Re}[e^{-ipr}e^{i\delta_{\kappa_i}}(s+i\eta) \times {}_1F_1(s+1+i\eta, 2s+1; 2ipr)],$$

$$f_{E\kappa_i}(r) = N_{\kappa_i}(|E|+1)^{\frac{1}{2}}(2pr)^{s-1}\mathrm{Im}[e^{-ipr}e^{i\delta_{\kappa_i}}(s+i\eta) \times {}_1F_1(s+1+i\eta, 2s+1; 2ipr)], \qquad (5)$$

with the parameters

$$p = \sqrt{E^2-1}, \quad \eta = \frac{\zeta E}{p}, \quad \delta_{\kappa_i} = \frac{1}{2}\arg\left(\frac{-\kappa_i + i\eta/E}{s+i\eta}\right),$$

$$\zeta = \alpha Z, \quad s = \sqrt{\kappa_i^2 - \zeta^2}, \quad N_{\kappa_i} = 2\sqrt{\frac{p}{\pi}}e^{\pi\eta/2}\frac{|\Gamma(s+i\eta)|}{\Gamma(2s+1)}. \qquad (6)$$

For more details, see [21,22].

So far, we have considered the initial- and final-state electron wave functions. The evaluation of the transition matrix element (1) also requires knowledge about the electron-photon interaction operator $\hat{R} = \boldsymbol{\alpha} \cdot \hat{\boldsymbol{u}}_\lambda e^{i\boldsymbol{k}\cdot\boldsymbol{r}}$. It is convenient to expand this operator in terms of the multipole components of the electromagnetic field [23]. For light propagating in the z direction, this expansion reads as

$$\hat{R} = \boldsymbol{\alpha} \cdot \hat{\boldsymbol{u}}_\lambda e^{ikz} = \sqrt{2\pi}\sum_{L=1}^{\infty}\sum_{p=0}^{1} i^L\sqrt{2L+1}\left[(i\lambda)^p\boldsymbol{\alpha}\cdot\boldsymbol{a}_{L\lambda}^{(p)}\right], \qquad (7)$$

where $\boldsymbol{a}_{L\lambda}^{(0)}$ and $\boldsymbol{a}_{L\lambda}^{(1)}$ are the magnetic and electric multipole fields with angular momentum L. Moreover, $\lambda = \pm 1$ is the photon helicity.

Having discussed all the components of Eq. (1), we can further evaluate the transition matrix element $M_{m_s\mu_f}(\lambda)$. By inserting the wave functions (2) and (3) into Eq. (1) we find

$$M_{m_s\mu_f}(\lambda) = \sum_{\kappa_i\mu_i} i^{l_i}e^{i\Delta_{\kappa_i}}\sqrt{4\pi(2l_i+1)}\left\langle l_i 0 \frac{1}{2} m_s \middle| j_i m_s \right\rangle$$
$$\times D_{\mu_i m_s}^{j_i}(\phi,\theta,0)\langle n_f\kappa_f\mu_f|\boldsymbol{\alpha}\cdot\hat{\boldsymbol{u}}_\lambda e^{ikz}|E\kappa_i m_s\rangle, \qquad (8)$$

where

$$\langle n_f\kappa_f\mu_f|\boldsymbol{\alpha}\cdot\hat{\boldsymbol{u}}_\lambda e^{ikz}|E\kappa_i m_s\rangle$$
$$= \frac{i}{\sqrt{2}}\left[\int d^3\boldsymbol{r}\, e^{i\boldsymbol{k}\cdot\boldsymbol{r}}g_{n_f\kappa_f}(r)\left(\chi_{\kappa_f}^{\mu_f}\right)^\dagger(\sigma_x + i\lambda\sigma_y)f_{E\kappa_i}(r)\chi_{-\kappa_i}^{\mu_i}\right.$$
$$\left.- \int d^3\boldsymbol{r}\, e^{i\boldsymbol{k}\cdot\boldsymbol{r}}f_{n_f\kappa_f}(r)\left(\chi_{-\kappa_f}^{\mu_f}\right)^\dagger(\sigma_x + i\lambda\sigma_y)g_{E\kappa_i}(r)\chi_{\kappa_i}^{\mu_i}\right]. \qquad (9)$$

With the aid of the Wigner-Eckart theorem along with the multipole expansion (7), and after performing some simple algebra, we finally obtain

$$M_{m_s\mu_f}(\lambda) = \sqrt{8\pi^2}\sum_{\kappa_i\mu_i Lp} i^{l_i+L}e^{i\Delta_{\kappa_i}}\sqrt{\frac{2l_i+1}{2j_f+1}}\sqrt{2L+1}$$
$$\times \left\langle l_i 0 \frac{1}{2} m_s \middle| j_i m_s \right\rangle\langle j_i\mu_i L\lambda | j_f\mu_f\rangle D_{\mu_i m_s}^{j_i}(\phi,\theta,0)$$
$$\times (i\lambda)^p\langle n_f\kappa_f\|\boldsymbol{\alpha}\cdot\boldsymbol{a}_L^{(p)}\|E\kappa_i\rangle. \qquad (10)$$

Here, $\langle n_f\kappa_f\|\boldsymbol{\alpha}\cdot\boldsymbol{a}_L^{(p)}\|E\kappa_i\rangle$ is the so-called reduced matrix element which is independent of the underlying geometry. It contains information about the electronic wave functions and is the central building block from which we calculate all properties of the process.

B. Differential cross sections and polarization parameters

In the previous section we discussed the evaluation of the transition matrix element (1). With the help of this matrix element we can now analyze the angular and polarization properties of bound-free pair production. In particular, the angle-differential cross section of the process is obtained as

$$\frac{d\sigma_{m_s\mu_f}}{d\Omega}(\lambda) = \frac{\alpha}{4k}\big|M_{m_s\mu_f}(\lambda)\big|^2, \tag{11}$$

where α is the fine-structure constant. Moreover, we have assumed that the incident light has a well defined helicity λ and the angular momentum projections of the outgoing positron and bound electron are observed. From cross section (11), one can evaluate observables for all possible scenarios of pair production. For example, if the positron spin state remains unobserved in an experiment, the cross section is obtained by performing the summation over m_s, $d\sigma_{\mu_f} = \sum_{m_s} d\sigma_{m_s\mu_f}$. If, in contrast, no information about the magnetic sublevel population of the residual hydrogenlike ions is available, the cross section reads as $d\sigma_{m_s} = \sum_{\mu_f} d\sigma_{m_s\mu_f}$. Finally, if neither electron nor positron angular momentum projections are detected, we obtain the cross section

$$\frac{d\sigma}{d\Omega}(\lambda) = \sum_{m_s\mu_f} \frac{d\sigma_{m_s\mu_f}}{d\Omega}(\lambda). \tag{12}$$

Again, for all scenarios above, we assumed that the incident light is circularly polarized and hence has a well defined helicity λ.

By using the differential cross sections introduced in this section, one can also calculate the degree of longitudinal polarization of the outgoing positrons and final hydrogenlike ions. For example, in a realistic experimental scenario in which the magnetic sublevel population of the ions remains unobserved, the degree of polarization of the positrons is given by

$$P_{\text{pos}}(\theta) = \frac{d\sigma_{m_s=\frac{1}{2}} - d\sigma_{m_s=-\frac{1}{2}}}{d\sigma_{m_s=\frac{1}{2}} + d\sigma_{m_s=-\frac{1}{2}}}. \tag{13}$$

Vice versa, the polarization of the hydrogenlike ions along the z axis reads as

$$P_{\text{ion}}(\theta) = \frac{d\sigma_{\mu_f=\frac{1}{2}} - d\sigma_{\mu_f=-\frac{1}{2}}}{d\sigma_{\mu_f=\frac{1}{2}} + d\sigma_{\mu_f=-\frac{1}{2}}}, \tag{14}$$

where we assumed a positron detector that is insensitive to the spin state.

III. COMPUTATIONAL DETAILS

The evaluation of matrix elements for bound-free transitions has been discussed many times in the literature, not only in the context of pair production but also for the photoelectric effect [24,25], radiative recombination [26], or single photon annihilation [27]. For this reason, we restrict our discussion of the computational details to just a brief overview. As already mentioned above, the main building block of our analysis is the reduced matrix element in Eq. (10) which corresponds to either an magnetic ($p = 0$) or electric ($p = 1$) transition. The

magnetic matrix element can be written as

$$\langle n_f\kappa_f\|\boldsymbol{\alpha}\cdot\boldsymbol{a}^{(0)}_{L\lambda}\|E_i\kappa_i\rangle = i(I_{1,L}\langle\kappa_f\|[\boldsymbol{Y}_L\otimes\boldsymbol{\sigma}]_L\|-\kappa_i\rangle$$
$$-\,I_{2,L}\langle-\kappa_f\|[\boldsymbol{Y}_L\otimes\boldsymbol{\sigma}]_L\|\kappa_i\rangle), \tag{15}$$

while the electric matrix element reads as

$$\langle n_f\kappa_f\|\boldsymbol{\alpha}\cdot\boldsymbol{a}^{(1)}_{L\lambda}\|E_i\kappa_i\rangle$$
$$= i\sqrt{\frac{L+1}{2L+1}}(I_{1,L-1}\langle\kappa_f\|[\boldsymbol{Y}_{L-1}\otimes\boldsymbol{\sigma}]_L\|-\kappa_i\rangle$$
$$-\,I_{2,L-1}\langle-\kappa_f\|[\boldsymbol{Y}_{L-1}\otimes\boldsymbol{\sigma}]_L\|\kappa_i\rangle)$$
$$-\,i\sqrt{\frac{L}{2L+1}}(I_{1,L+1}\langle\kappa_f\|[\boldsymbol{Y}_{L+1}\otimes\boldsymbol{\sigma}]_L\|-\kappa_i\rangle$$
$$-\,I_{2,L+1}\langle-\kappa_f\|[\boldsymbol{Y}_{L+1}\otimes\boldsymbol{\sigma}]_L\|\kappa_i\rangle). \tag{16}$$

The angular part of these matrix elements is given by the reduced matrix element of the operator $[\boldsymbol{Y}_L\otimes\boldsymbol{\sigma}]_L$ and can be calculated analytically using the standard Racah algebra [28]. The radial parts $I_{1,L}$ and $I_{2,L}$ contain the integrals of the radial components of the electron and positron wave functions along with the spherical Bessel function of order L. Its numerical calculation is usually a rather complicated task. However, for e^-e^+ pair production in collisions of photons with initially bare ions, the radial components are known analytically [21]. In this case, the exact solution of the radial integrals can be given in terms of Gaussian hypergeometric functions [2] which we calculate numerically using the Arb C library [29].

As seen from Eq. (10) the reduced matrix elements for various positron and photon multipoles, κ_i and L, contribute to $M_{m_s\mu_f}(\lambda)$. Since we consider a high energy atomic process a sufficiently large number of these partial waves have to be taken into account to achieve convergence of the cross section. For example, for $E_+ = 10\,m_ec^2$ our results contain partial waves up to $|\kappa_i| = 140$.

IV. RESULTS AND DISCUSSION

A. Differential cross sections

With the help of Eqs. (10)–(14) we are now ready to investigate e^-e^+ bound-free pair production in photon-ion interactions. We start our analysis with the angle-differential cross sections which we calculate for photons with helicity $\lambda = +1$ colliding with bare hydrogen and lead ions. For both targets we focus on the capture of the produced electrons into the ground $1s_{1/2}$ ionic state and consider low and high energy regimes corresponding to positron energies of $E_+ = 1.5\,m_ec^2$ and $E_+ = 10\,m_ec^2$, respectively. Moreover, we discuss different "polarization scenarios" in which the angular momentum projections of either the final hydrogenlike ions or emitted positrons are observed. In Fig. 1 for example, we display the differential cross section $d\sigma_{m_s} = \sum_{\mu_f} d\sigma_{m_s\mu_f}$ which is obtained upon summation over the final ionic states but in which the positron helicity is fixed to $m_s = +1/2$ (red dashed line) or $m_s = -1/2$ (blue dotted line). The sum of the two helicity contributions $d\sigma = \sum_{m_s} d\sigma_{m_s}$ is displayed by the black solid line. As seen from the figure, this summed angle-differential cross section $d\sigma$ behaves in a rather different way for light (hydrogen) and heavy (lead) target ions. In particular, while for $Z = 82$ the maximum of positron emission is in
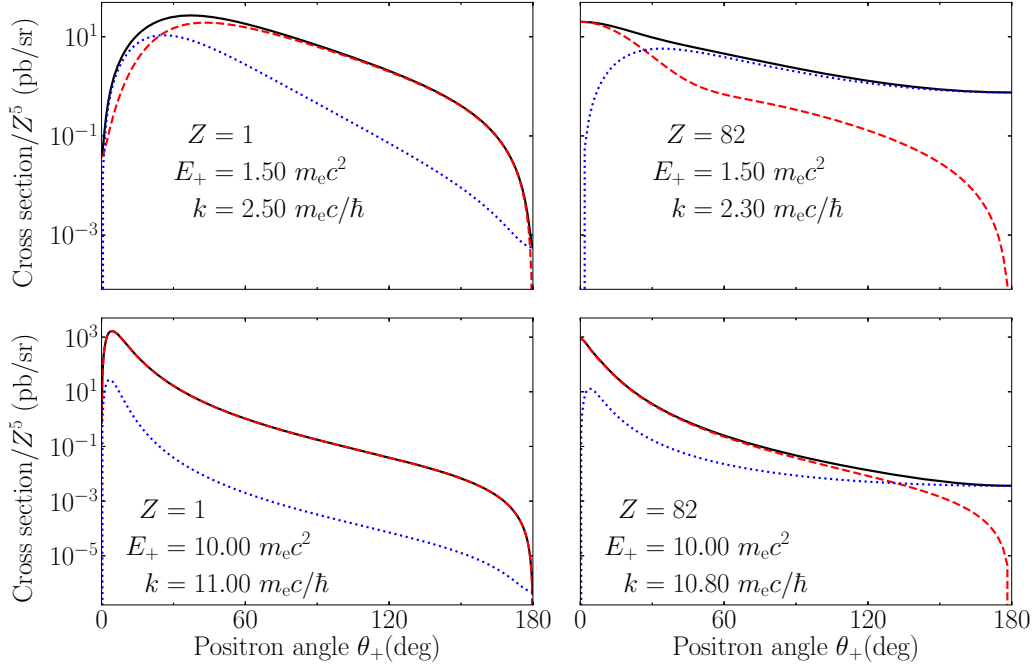
FIG. 1. Differential cross sections for bound-free e^-e^+ pair production in collisions of photons with helicity $\lambda = +1$ and bare hydrogen (left panels) and lead (right panels) ions. Calculations have been performed for positron energies $E_+ = 1.5\, m_e c^2$ (upper panels) and $E_+ = 10\, m_e c^2$ (lower panels) and for capture of the electron in the ground ionic state. Moreover, three scenarios are considered in which the spin projection of the emitted positrons either remains unobserved (black solid line) or is fixed to $m_s = +1/2$ (red dashed line) or $m_s = -1/2$ (blue dotted line). The photon and positron energies in the legend are rounded to two decimal places.

the forward direction, $\theta_+ = 0°$, it is shifted to higher angles θ_+ for $Z = 1$. For example, for positrons with energy $E_+ = 1.5\, m_e c^2$, the differential cross section $d\sigma$ has its maximum at $\theta_+ \approx 37°$. This behavior has been previously predicted within the framework of the relativistic Born approximation in which the outgoing positron is treated as a plane wave [16,24,30,31]. The Born approximation also suggests the drastic suppression of positron emission in the forward and backward directions in the low-Z regime; this can be clearly observed in the left panels of Fig. 1.

The angular distribution of the emitted positrons also depends on their helicity m_s. It is particularly easy to see the effect for the lead target, for which the forward emission is dominated by positrons with helicity $m_s = +1/2$ while positrons with $m_s = -1/2$ are most likely emitted under large angles. This behavior can be understood based on the analysis of the angular momentum projections for the two ultimate cases $\theta_+ = 0°$ and $\theta_+ = 180°$, i.e., for propagation of the positron either parallel or antiparallel to the z axis. For these two cases the spin projections of the bound-electron and emitted positron should add up to the helicity of the incident photon,

$$\lambda = \mu_f + \widetilde{m}_s. \tag{17}$$

Here, $\widetilde{m}_s$ is *not* the helicity but the projection of the positron spin on the z axis. If the electron is captured into the ground ionic state, its angular momentum projection can be $\mu_f = \pm 1/2$. Therefore, only the combination $\mu_f = +1/2$ and $\widetilde{m}_s = +1/2$ can compensate the helicity $\lambda = +1$; see Eq. (17). However, as we already mentioned above, $\widetilde{m}_s$ is the projection of the positron spin on the direction of the incident light,

which is related to the helicity as $m_s = \widetilde{m}_s = +1/2$ for $\theta_+ = 0°$ and $m_s = -\widetilde{m}_s = -1/2$ for $\theta_+ = 180°$.

Until now we have discussed the differential cross section for bound-free pair production under the assumption that the spin state of the final hydrogenlike ions remains unobserved. In order to investigate how the probability of the e^-e^+ process depends on the magnetic sublevel population of the residual ions, we display in Fig. 2 the differential cross section $d\sigma_{\mu_f} = \sum_{m_s} d\sigma_{m_s \mu_f}$ for $\mu_f = +1/2$ (red dashed line) and $\mu_f = -1/2$ (blue dotted line). This cross section has been obtained upon summation over the positron spin states and for incident photons with helicity $\lambda = +1$. Similar to before, calculations have been performed for hydrogen and lead ions as well as for positron energies $E_+ = 1.5\, m_e c^2$ and $E_+ = 10\, m_e c^2$. As seen from the figure, for both energies and targets, and nearly for all emission angles, the e^-e^+ process leads almost exclusively to the production of hydrogenlike ions with the magnetic quantum number $\mu_f = +1/2$. To explain this effect one has to revisit Eq. (9) in which the matrix element $\langle n_f \kappa_f \mu_f | \boldsymbol{\alpha} \cdot \hat{\boldsymbol{u}}_\lambda e^{ikz} | E\kappa_i m_s \rangle$ is written as the sum of two integrals. The first integral contains the product of the upper electron $g_{n_f \kappa_f}$ and lower positron $f_{E\kappa_i}$ components. In contrast, the product of the lower electron $f_{n_f \kappa_f}$ and upper positron $g_{E\kappa_i}$ functions can be found under the second integral. For moderate relativistic energies the contribution of this second integral to the matrix element is negligible since both $f_{n_f \kappa_f}$ and $g_{E\kappa_i}$ are *small* components. Therefore, the behavior of the differential cross is mainly determined by the first term in Eq. (9) which includes the *large* electron and positron components. However, the angular part of this integral $(\chi_{\kappa_f}^{\mu_f})^\dagger (\sigma_x + i\lambda\sigma_y) \chi_{-\kappa_i}^{\mu_i}$ vanishes for $\mu_f = -1/2$
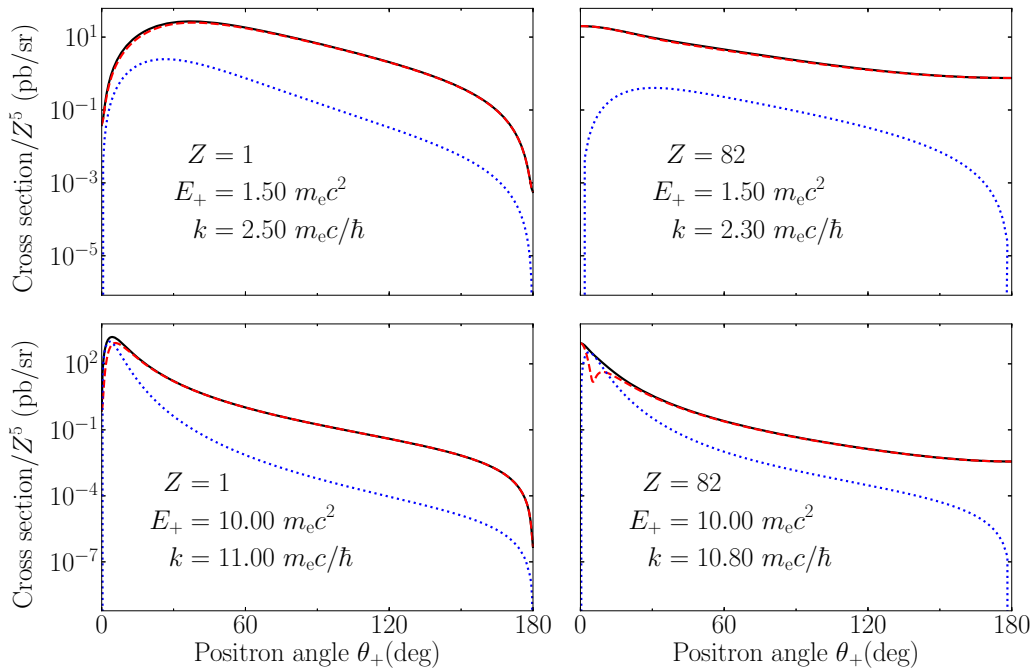
FIG. 2. As in Fig. 1 but for well defined magnetic quantum numbers $\mu_f = +1/2$ (red dashed line) and $\mu_f = -1/2$ (blue dotted line) of the bound-state electron while the positron spin state remains unobserved. As before, the black solid line represents the summed partial differential cross section.

and $\lambda = +1$. This matches our observation from Fig. 2 of the strongly suppressed production of ions with $\mu_f = -1/2$. As seen from Eq. (5), for very high energies $|E| \gg 1$ the upper and lower components of the positron wave function become comparable which leads to the enhancement of the contribution of the second integral in Eq. (9). This integral does not disappear for $\lambda = +1$ and $\mu_f = -1/2$ and can result in a significant contribution of $d\sigma_{\mu_f = -1/2}$. As seen from the lower panels of Fig. 2, this partial cross section even becomes dominant for a small range of emission angles around $\theta_+ \approx 2.5°$ for $Z = 1$ and $\theta_+ \approx 6.5°$ for $Z = 82$.

The results presented in this section have been obtained under the assumption that the target nucleus is infinitely heavy and pointlike. One has to estimate, therefore, how the nuclear recoil and finite size affect the pair production cross sections and polarization parameters. The recoil effect can be accounted for in first order by altering the energy of the emitted positron according to the laws of energy and momentum conservation. Calculations with such an adjusted energy show that the change in the angle-differential cross section is usually on the subpercent level. Even in the worst case of backward positron emission for a high photon energy $E_{ph} = 11 m_e c^2$ and hydrogen target ions, the change in the cross section is only around 4%. We furthermore argue that nuclear size effects do not play a significant role for bound-free pair production in the parameter regime studied in the present work since the corresponding effects for the very similar process of radiative recombination are also on the subpercent level [32]. The influence of these two effects is therefore expected to be below the accuracy of modern positron detectors.

B. Degree of polarization

As we discussed in the previous section, the process of bound-free pair production is very sensitive to the spin state of the emitted positrons and residual hydrogenlike ions. In order to investigate this m_s and μ_f dependence in detail, it is convenient to analyze not only the partial differential cross sections but also the degrees of positron and ion polarization, Eqs. (13) and (14). Similar to before, we start with the emitted positrons, whose degree of polarization $P_{pos}(\theta_+)$ is displayed in Fig. 3. To be consistent with the results of the previous section, calculations have been performed for collisions of photons with helicity $\lambda = +1$ with bare hydrogen and lead ions as well as for positron energies $E_+ = 1.5 m_e c^2$, $E_+ = 5 m_e c^2$, and $E_+ = 10 m_e c^2$. Moreover, $P_{pos}(\theta_+)$ has been obtained under the assumption that the spin state of the hydrogenlike ions remains unobserved. As seen from the figure, $P_{pos}(\theta_+) \approx +1$ for $\theta_+ \to 0°$, implying that for the forward emission positrons are strongly polarized in the direction of propagation. In contrast, for larger angles θ_+ the degree of polarization decreases and reaches the value $P_{pos}(\theta_+) = -1$ for $\theta_+ = 180°$; the effect which can be expected from Eq. (17). The behavior of $P_{pos}(\theta_+)$ between the two ultimate angles $\theta_+ = 0°$ and $\theta_+ = 180°$ strongly depends on the positron energy and charge of the target ion. For very high relativistic energies, for example, the creation of positrons with helicity $m_s = +1/2$ remains dominant in a rather large angular range. This effect is most pronounced for hydrogen ions and positron energies of $E_+ = 10 m_e c^2$ for which $P_{pos}(\theta_+) \approx +1$ for $0° \leqslant \theta_+ \lesssim 178°$.

One may note from Fig. 3 that our results for the degree of positron polarization differ from those of Agger and Sørensen [16]. The reason for this disagreement is the choice of the
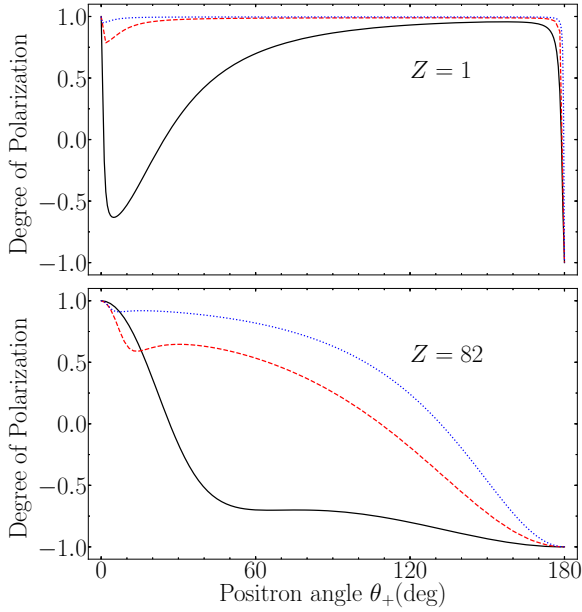
FIG. 3. Degree of polarization of the created positrons (13) for bound-free $e^- e^+$ pair production in collisions of photons with helicity $\lambda = +1$ and bare hydrogen (upper panel) and lead (lower panel) ions. Calculations have been performed for positron energies $E_+ = 1.5\, m_e c^2$ (black solid line), $E_+ = 5\, m_e c^2$ (red dashed line), and $E_+ = 10\, m_e c^2$ (blue dotted line) and for capture of the electron into the ground $1s_{1/2}$ ionic state.
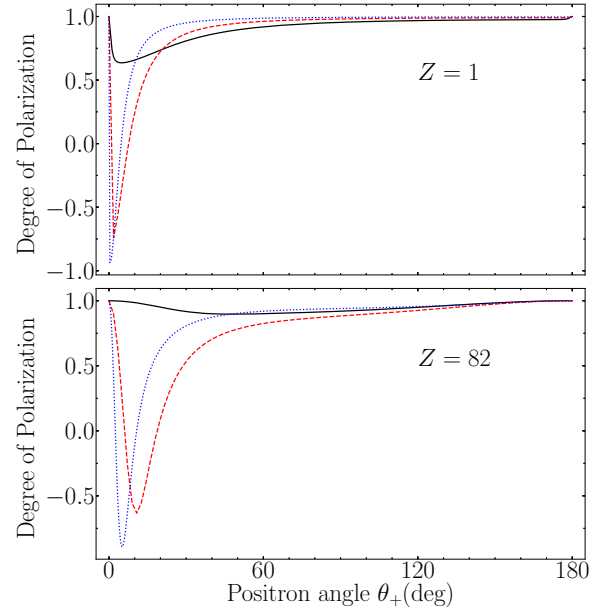
axis with respect to which the spin of the created positrons is quantized. In Ref. [16] this axis was chosen along the propagation direction of the incident light. However, this choice is insufficient to analyze the polarization effects in pair production because for relativistic particles the only direction along which one can uniquely define polarization is their own direction of propagation. Therefore, one has to define the partial differential cross sections in Eq. (13) in the helicity basis, i.e., with respect to the asymptotic momentum of the created positrons $\boldsymbol{p}_+$. Such calculations are shown in Fig. 3.

Besides the emitted positrons it is also instructive to analyze the degree of polarization of the produced hydrogenlike ions $P_{\mathrm{ion}}(\theta_+)$. It is obtained from Eq. (14), where the magnetic quantum number μ_f is defined with respect to the propagation direction of the incident light. Predictions for $P_{\mathrm{ion}}(\theta_+)$ are presented in Fig. 4 for the same set of parameters as used above for the positron polarization. The figure clearly indicates that for positron emission in the forward and backward direction the hydrogenlike ions are always produced in the magnetic substate $|1s_{1/2}, \mu_f = +1/2\rangle$. Moreover, almost exclusive population of the state with $\mu_f = +1/2$ can be observed for relatively low positron energies (see black solid line). Only in the strongly relativistic regime, the predominant population of the sublevel with $\mu_f = -1/2$ becomes possible in a rather restricted range of forward emission angles. For example for $E_+ = 10\, m_e c^2$, the partial cross section $d\sigma_{\mu_f = -1/2}$ is dominant for the range $0.2° \lesssim \theta_+ \lesssim 4.7°$ for $Z = 1$ and $2.5° \lesssim \theta_+ \lesssim 10.7°$ for $Z = 82$. A detailed explanation of this effect based on the analysis of Eq. (9) was given in the previous section. The results of our calculations, therefore, indicate

FIG. 4. Degree of polarization of the residual hydrogenlike ions (14) for the same parameters as in Fig. 3.

that bound-free pair production by circularly polarized light may be used to produce hydrogenlike ions with a high degree of longitudinal polarization.

C. Transformation into the laboratory frame

So far we have considered bound-free pair production under the assumption that the positron is detected in the rest frame of the ion. In storage ring experiments, however, the ions are usually moving with high relativistic velocities. Of course our theory can be also applied to predict the outcome of such experiments if an appropriate transformation is applied.
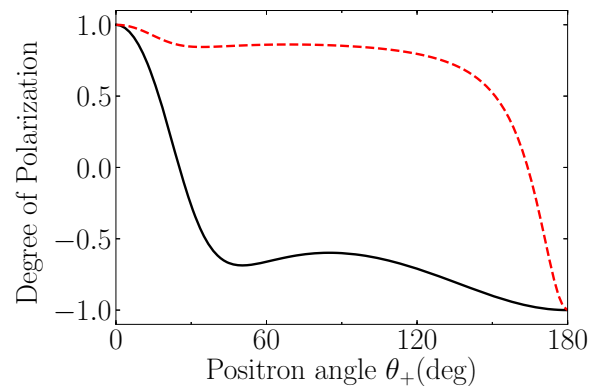

FIG. 5. Degree of polarization of the created positrons (13) for bound-free $e^- e^+$ pair production in head-on collisions of photons with helicity $\lambda = +1$ and bare lead ions. Calculations have been performed for a photon energy $E_{\mathrm{ph}} = 2.30\, m_e c^2$ and for capture of the electron into the ground $1s_{1/2}$ ionic state. The target ion is moving with a Lorentz factor of $\gamma = 1.01$ (black solid line) or $\gamma = 2.00$ (red dashed line). θ_+ is defined with respect to the propagation direction of incident light.

The Lorentz transformation from the projectile frame (primed variables) to the laboratory frame (unprimed variables) reads as

$$\frac{\sin\theta'_+}{\sin\theta_+} = \sqrt{\gamma^2(g+\cos\theta'_+)^2 + \sin^2\theta'_+}, \quad (18)$$

$$\frac{d\sigma}{d\Omega} = \left|\frac{d\cos\theta'_+}{d\cos\theta_+}\right|\frac{d\sigma'}{d\Omega'}, \quad (19)$$

where $g = \beta/\beta'$ is the ratio of the reduced velocities of the ion and the positron in the projectile frame. For more details see [21]. Just as an example we present in Fig. 5 the degree of positron polarization in the laboratory frame for head-on collisions of photons with helicity $\lambda = +1$ and energy $E_{\rm ph} = 2.30\, m_e c^2$ with bare lead ions. The ions are moving with a Lorentz factor of either $\gamma = 1.01$ or $\gamma = 2.00$, which are typical velocities for the GSI and future FAIR facilities.

As seen from the figure, for the low Lorentz factor, the degree of polarization is almost identical to the low energy and high-Z case in Fig. 3. For higher relativistic velocities, the curve is altered by two effects: (i) The photon energy, as "seen" by the moving ion, is Doppler boosted, which is why the result resembles the ones for higher energies, and (ii) the emission angle is Lorentz transformed, causing a distortion of the angular distribution.

V. SUMMARY

In conclusion, we presented a theoretical study of bound-free electron-positron pair production in the interaction of γ rays with bare ions. Based on the rigorous solutions of the relativistic Dirac equation and by making use of the first-order perturbation theory for the electron-photon coupling, we studied the polarization properties of the created positrons and residual hydrogenlike ions. Calculations have been performed for circularly polarized photons in a wide range of energies and for low- and high-Z targets. Results of these calculations have clearly shown that in the relatively low energy regime, i.e., when $E_+ \approx m_e c^2$, the produced ions are strongly longitudinally polarized in the direction of the incident photon beam for all positron emission angles. In contrast, for high energies $E_+ \gg m_e c^2$ and emission close to the forward direction $\theta_+ = 0$, the ions are polarized opposite to the photon wave vector. Moreover, also the positron spin state strongly depends on the energy of the incident light and nuclear charge of the target. For example, for low-Z targets, ultrarelativistic energies, and an initial photon helicity of $\lambda = +1$, the positrons are almost exclusively created in the spin state with $m_s = +1/2$. We argue, therefore, that bound-free pair production can be used as a source of strongly polarized positrons and hydrogenlike ions; this effect is likely to be observed soon in the future FAIR facility in Darmstadt and in the Gamma Factory at CERN.

[1] M. Krasny, R. Alemany-Fernández, P. Antsifarov, A. Apyan, H. Bartosik, E. Bessonov, N. Biancacci, J. Bieron, D. Budker, K. Cassou, F. Castelli, I. Chaikovska, R. Chehab, C. Curatolo, P. Czodrowski, K. Dupraz, K. Dzierzega, B. Goddard, S. Hirlaender, J. Jowett *et al.*, The CERN Gamma Factory Initiative: An Ultra-High Intensity Gamma Source, in *Proceedings of the 9th International Particle Accelerator Conference, IPAC18*, April 29–May 4, Vancouver (JACoW, Geneva, 2018).

[2] I. Øverbø, K. Mork, and H. A. Olsen, Exact calculation of pair production, Phys. Rev. **175**, 1978 (1968).

[3] V. M. Budnev, I. F. Ginzburg, G. V. Meledin, and V. G. Serbo, The two-photon particle production mechanism. Physical problems. Applications. Equivalent photon approximation, Phys. Rep. **15**, 181 (1975).

[4] D. Yu. Ivanov, A. Schiller, and V. G. Serbo, Large Coulomb corrections to the e^+e^- pair production at relativistic heavy ion colliders, Phys. Lett. B **454**, 155 (1999).

[5] R. N. Lee, A. I. Milstein, and V. G. Serbo, Structure of the Coulomb and unitarity corrections to the cross section of e^+e^- pair production in ultrarelativistic nuclear collisions, Phys. Rev. A **65**, 022102 (2002).

[6] G. Baur, K. Hencken, and D. Trautmann, Electron-positron pair production in ultrarelativistic heavy ion collisions, Phys. Rep. **453**, 1 (2007).

[7] Brookhaven National Lab, Upton, NY (USA) (1989), Conceptual design of the Relativistic Heavy Ion Collider [RHIC] (BNL–52195), United States.

[8] R. Bruce, J. M. Jowett, S. Gilardoni, A. Drees, W. Fischer, S. Tepikian, and S. R. Klein, Observations of Beam Losses Due to Bound-Free Pair Production in a Heavy-Ion Collider, Phys. Rev. Lett. **99**, 144801 (2007).

[9] C. F. V. Weizsäcker, Ausstrahlung bei Stößen sehr schneller Elektronen, Z. Phys. **88**, 612 (1934).

[10] E. J. Williams, Nature of the high energy particles of penetrating radiation and status of ionization and radiation formulae, Phys. Rev. **45**, 729 (1934).

[11] Y. S. Tsai, Laser $+ e^- \rightarrow \gamma + e^-$ and laser $+ \gamma \rightarrow e^+ + e^-$ as sources of producing circularly polarized γ and $e^\pm$ beams, Phys. Rev. D **48**, 96 (1993).

[12] D. Yu. Ivanov, G. L. Kotkin, and V. G. Serbo, Complete description of polarization effects in e^+e^- pair production by a photon in the field of a strong laser wave, Eur. Phys. J. C **40**, 27 (2005).

[13] A. Di Piazza, A. I. Milstein, and C. Müller, Polarization of the electron and positron produced in combined Coulomb and strong laser fields, Phys. Rev. A **82**, 062110 (2010).

[14] T.-O. Müller and C. Müller, Longitudinal spin polarization in multiphoton Bethe-Heitler pair production, Phys. Rev. A **86**, 022109 (2012).

[15] A. Aste, K. Hencken, D. Trautmann, and G. Baur, Electromagnetic pair production with capture, Phys. Rev. A **50**, 3980 (1994).

[16] C. K. Agger and A. H. Sørensen, Pair creation with bound electron for photon impact on bare heavy nuclei, Phys. Rev. A **55**, 402 (1997).

[17] A. Belkacem and A. H. Sørensen, Bound-free heavy-lepton pair production for photon and ion impact on atomic nuclei, Phys. Rev. A **57**, 3646 (1998).

[18] A. Aste, Bound-free pair production cross-section in heavy-ion colliders from the equivalent photon approach, EPL (Europhysics Letters) **81**, 61001 (2008).

[19] C. Deneke and C. Müller, Bound-free e^+e^- pair creation with a linearly polarized laser field and a nuclear field, Phys. Rev. A **78**, 033431 (2008).

[20] A. N. Artemyev, U. D. Jentschura, V. G. Serbo, and A. Surzhykov, Bound-free pair production in ultra-relativistic ion collisions at the LHC collider: Analytic approach to the total and differential cross sections, Eur. Phys. J. C **72**, 1935 (2012).

[21] J. Eichler, *Relativistic Atomic Collisions* (Elsevier, Amsterdam, 1995).

[22] J. Eichler, *Lectures on Ion-Atom Collisions* (Elsevier, Amsterdam, 2005).

[23] M. E. Rose, *Elementary Theory of Angular Momentum* (Wiley, New York, 1957).

[24] R. H. Pratt, Atomic photoelectric effect at high energies, Phys. Rev. **117**, 1017 (1960).

[25] W. R. Alling and W. R. Johnson, Exact calculation of K-shell and L-shell photoeffect, Phys. Rev. **139**, A1050 (1965).

[26] A. Ichihara, T. Shirai, and J. Eichler, Radiative electron capture and the photoelectric effect at high energies, Phys. Rev. A **54**, 4954 (1996).

[27] L. Sodickson, W. Bowman, J. Stephenson, and R. Weinstein, Single-quantum annihilation of positrons, Phys. Rev. **124**, 1851 (1961).

[28] I. P. Grant, *Relativistic Quantum Theory of Atoms and Molecules: Theory and Computation*, Springer Series on Atomic, Optical, and Plasma Physics (Springer-Verlag, New York, 2007).

[29] F. Johansson, Arb: Efficient arbitrary-precision midpoint-radius interval arithmetic, IEEE Trans. Comput. **66**, 1281 (2017).

[30] H. J. Bhabha, H. R. Hulme, and F. R. Howard, The annihilation of fast positrons by electrons in the K-shell, Proc. R. Soc. London, Ser. A **146**, 723 (1934).

[31] W. R. Johnson, Angular distribution of single-quantum annihilation radiation, Phys. Rev. **159**, 61 (1967).

[32] J. Holmberg, A. N. Artemyev, A. Surzhykov, V. A. Yerokhin, and Th. Stöhlker, QED corrections to radiative recombination and radiative decay of heavy hydrogenlike ions, Phys. Rev. A **92**, 042510 (2015).